Contrib Mineral Petrol (2002) 142: 700–713
DOI 10.1007/s00410-001-0319-4

Yaron Katzir · John W. Valley · Alan Matthews
Michael J. Spicuzza

Tracking fluid flow during deep crustal anatexis: metasomatism of peridotites (Naxos, Greece)

Received: 19 March 2001 / Accepted: 26 September 2001 / Published online: 24 October 2001

Abstract Horizons of ultramafic lenses were metamorphosed with host felsic gneisses at upper amphibolite facies conditions during the M2 event on the island of Naxos, Greece. The synkinematic peak M2 Ol–Opx–Hbl–Chl–Spl assemblage of the Main, migmatite-associated, Ultramafic Horizon (MUH) retains mantle-like chemical and oxygen isotope compositions and thus shows no evidence of infiltration of fluids from the host rocks. A bimodal distribution of temperatures, grouped at 700 and 1,200 °C, is given by oxygen isotope Opx–Ol thermometry in the MUH meta-peridotites and indicates partial oxygen exchange during M2 superposed over previous mantle fractionation. The Agia Ultramafic Horizon (AUH), a coarser-grained and unfoliated peridotite, occurs within sillimanite gneisses in northwest Naxos and contains talc–enstatite and olivine domains. Recrystallization of the AUH peridotite during post-peak M2 infiltration of silica-rich, high $\delta^{18}O$ fluids is indicated by lack of deformation, increased activity of silica required to stabilize the talc–enstatite assemblage, extremely high $\delta^{18}O$ values of Ol and Opx and $\Delta^{18}O_{(Opx–Ol)}$ temperatures of 520–650 °C. The source for these fluids is inferred to be aplitic and pegmatitic dikes emanating from the migmatitic core of Naxos and intruding the AUH. At peak M2 temperatures and during anatexis of gneisses, volumes of fluid were small and fluid composition was locally buffered in the deeper part of the Naxos section. Crystallization of melts within the migmatitic core released siliceous fluids and initiated an episode of retrograde hydrous metamorphism in the overlying sequences, as observed in the AUH.

Y. Katzir (✉) · J.W. Valley · M.J. Spicuzza
Department of Geology and Geophysics,
University of Wisconsin, 1215 W. Dayton St.,
Madison, WI 53706, USA
E-mail: yaron@geology.wisc.edu
Tel.: +1-608-2627118
Fax: +1-608-2620693

A. Matthews
Institute of Earth Sciences,
The Hebrew University of Jerusalem,
Jerusalem, 91904, Israel

Editorial responsibility: J. Hoefs

Introduction

Fluid flow during prograde metamorphism of surface-derived rocks can be driven by the release of water-rich fluids during dehydration reactions. However, at high metamorphic grade, silicate melts may act as a temporary volatile sink for hydrous fluids. At the onset of melting, silicate liquids can dissolve aqueous fluids resulting in the formation of "dry" anatectic gneisses (Fyfe 1973; Lamb and Valley 1984; Valley et al. 1990; Spear et al. 1999). As temperatures decrease, melts crystallize and volatiles will be released, providing a source of retrograde fluids. The inevitability of a late retrograde phase of fluid flow and re-hydration in migmatitic terrains is predicted by experiments and models of crustal anatexis (Stevens et al. 1997; Clemens and Droop 1998; Spear et al. 1999) and fluid inclusion, petrologic, and stable isotope evidence for this process has been recognized in a number of field-based studies (Olsen 1987; Cartwright 1988; Baker et al. 1989; Buick et al. 1997; Kohn et al. 1997; Matthews et al. 2002, unpublished).

A prerequisite for understanding metamorphic fluid–rock interaction accompanying volatile release from crystallizing melts is isolating the compositional effect caused by the infiltrating fluids from pre- and syn-metamorphic chemical and isotopic variations. Ultramafic rocks are potentially sensitive recorders of such processes since they contain assemblages highly sensitive to siliceous fluids and their initial oxygen isotope ratios are distinctly lower than those of felsic rocks. However, ultramafic rocks may also experience pre-metamorphic serpentinization, which could raise their isotopic ratios and silica contents. Retrograde infiltration of fluids expelled from crystallizing granitic melts

should thus be most clearly seen in pristine, unaltered ultramafic rocks.

This study focuses on the island of Naxos (Cyclades, Greece; Fig. 1), where anatexis and migmatization occurred in the structurally deepest rocks during an Early Miocene high-temperature metamorphic event (M2) (Jansen and Schuiling 1976; Andriessen et al. 1979; Buick 1988; Wijbrans and McDougall 1988). Petrologic, textural, and stable isotopic evidence from marble intercalations within the migmatite core (leucogneiss core) and overlying sillimanite–gneisses and schists (Lower Series) indicates retrograde infiltration of hydrous fluids derived from crystallization of partial melts (Baker et al. 1989; Baker and Matthews 1994, 1995; Matthews et al. 2002). In this study, we present a petrologic and oxygen isotope study of ultramafic horizons that occur at the leucogneiss core–Lower Series boundary and within the Lower Series. The ultramafic rocks were incorporated into the subducted continental margin sequence of Naxos at depth during Eocene high-pressure metamorphism (M1) and underwent high-temperature Barrovian metamorphism (M2) along with their host rocks during exhumation (Katzir et al. 1999). The ultramafic assemblages and their initial whole-rock oxygen isotope composition, which is distinct from that of the host rocks, make them potentially excellent recorders of mass transport on Naxos. From these assemblages we constrain the timing and scale of episodes of fluid flow, and the composition and mode of transport of fluids during crustal anatexis and M2 metamorphism on Naxos.

Oxygen isotope compositions of minerals from mantle xenoliths are widely applied to mantle geothermometry or as indicators of metasomatic processes (Kyser et al. 1981, 1982; Gregory and Taylor 1986). The $\delta^{18}O$ values of mantle minerals and mantle-derived magmas have been shown to be largely homogenous (Mattey et al. 1994a; Eiler et al. 1996; Valley et al. 1998; Deines and Haggerty 2000), thus allowing new empirical

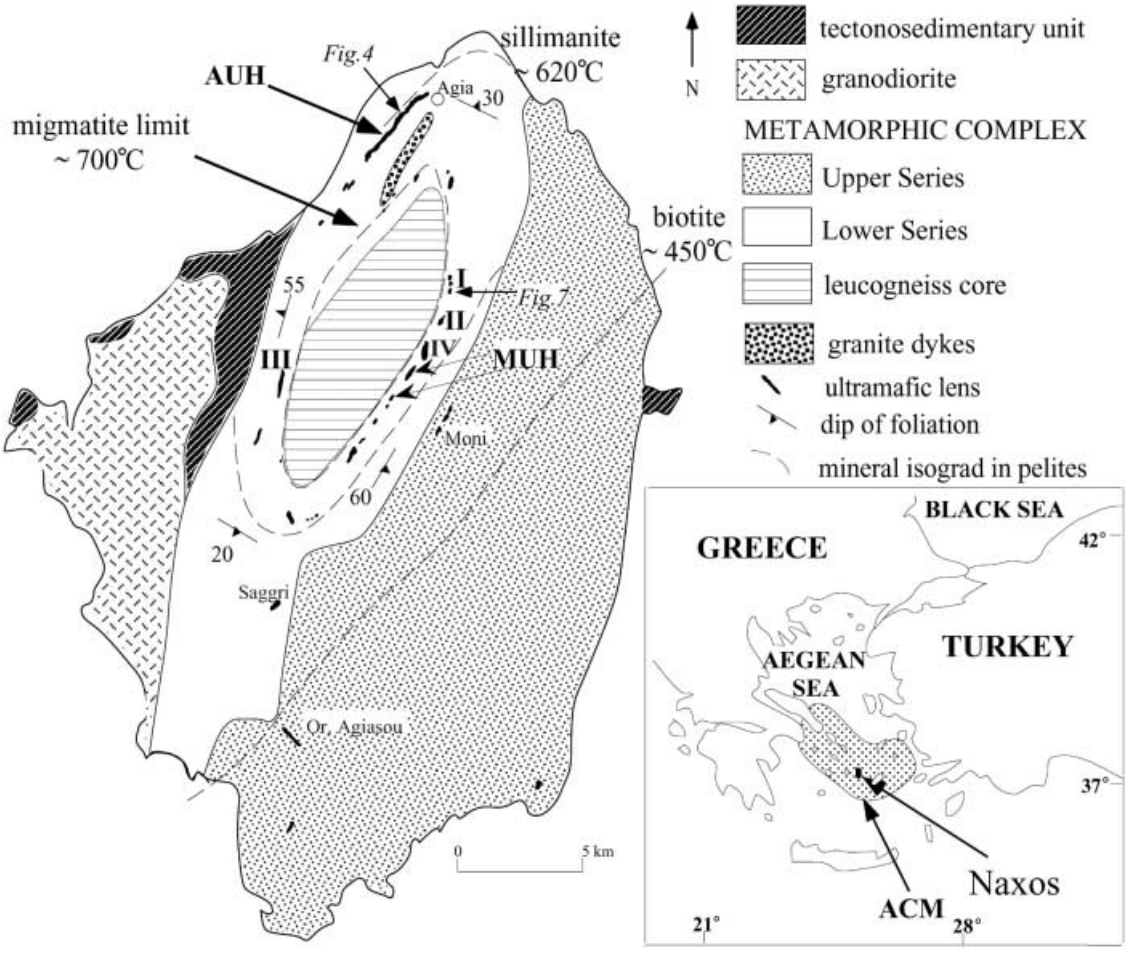

Fig. 1 A simplified geological map of Naxos after Jansen and Schuiling (1976) and Baker and Matthews (1994) showing the metamorphic complex (subdivided), the granodiorite and the tectonosedimentary unit. Ultramafic rocks (in *black*) occur within the metamorphic dome in four different structural levels: (1) at the contact of the leucogneiss core with the overlying Lower Series (the Main Ultrabasic Horizon *MUH*). *Roman numerals* show the positions of the key outcrops which are described in the text: *I* Koronos; *II* Keramoti; *III* Kourounochorio; *IV* Kinidharos; (2) Agia Ultrabasic Horizon (*AUH*) within the Lower Series; (3) at the contact between the Lower and Upper Units (Moni and Saggri exposures); (4) within the Upper Series (Ormos Agiasou exposure). The M2 mineral isograds mapped by Jansen and Schuiling (1976) and modified by Feenstra (1985) and Buick (1988) are shown. *ACM* Attic Cycladic Massif

calibration of isotopic fractionations. The experimental oxygen isotope olivine–orthopyroxene thermometer was calibrated at 1,000–1,300 °C (Rosenbaum et al. 1994). We apply these empirical and experimental isotopic calibrations to Naxos ultramafics, metamorphosed at upper amphibolite facies conditions, thus testing their accuracy under crustal conditions.

Analytical methods – stable isotopes

Mineral separates (1–2 mg per analysis) were hand-picked from crushed and sieved rock samples. Minerals were distinguished under a binocular and a petrographic microscope according to their texture, color, grain size, and habit. A large effort was made to avoid altered or inclusion-bearing grains resulting in high-purity (~99%) separates. The mineral chemistry of representative grains was determined using EPMA.

Oxygen isotope analyses were performed using the laser fluorination technique at the University of Wisconsin-Madison. BrF_5 was used as the reagent. Oxygen was purified cryogenically and with an inline Hg diffusion pump, converted to CO_2 using a hot graphite rod, and analyzed on a Finnigan MAT 251 mass spectrometer (Valley et al. 1995). Quartz separates were analyzed using the rapid heating, defocused beam technique (Spicuzza et al. 1998a). Biotite, plagioclase, and chlorite separates, which might react appreciably with BrF_5 at room temperature, were analyzed using an ''air-lock'' sample chamber (Spicuzza et al. 1998b). Of the133 mineral separates analyzed, 23% were duplicated. Average reproducibilities for olivine and orthopyroxene are $\pm 0.12‰$ ($n=9$) and $\pm 0.09‰$ ($n=4$), respectively. On each of the 15 analysis days at least four aliquots of UW Gore Mountain Garnet standard (UWG-2) were analyzed. The overall average for 78 analyses of UWG-2 in this study is $5.72 \pm 0.15‰$ ($1SE = \pm 0.02‰$). Data from each day of analysis were adjusted by an average of $0.10‰$, determined by the difference between each day's UWG-2 value and $5.8‰$ (SMOW), the accepted $\delta^{18}O$ value of UWG-2. NBS-28 African Glass Sand analyzed during this work yielded $9.46 \pm 0.09‰$ ($n=3$, corrected).

Regional geological setting

The Attic–Cycladic Massif (Fig. 1) records an Alpine orogenic cycle of collisional thickening, collapse, and reworking by back-arc extension (Avigad et al. 1997). This cycle is well represented by the geological evolution of Naxos (central Cyclades) where an Early Miocene Barrovian-type overprint (M2) occurred during extension and exhumation of former high-P rocks and almost totally obliterated M1 assemblages and fabrics.

Naxos is a mantled gneiss dome. The leucogneiss core (Buick 1988) consists of migmatites formed during M2 metamorphism of pre-Alpine basement (Andriessen et al. 1987; Keay and Lister 1997; Reischmann 1998). Overlying the leucogneiss core is a 7-km-thick meta-sedimentary envelope dominated by siliciclastic schists and gneisses in its lower part (''Lower Series'' of Jansen and Schuiling 1976), and by meta-bauxite bearing marbles in its upper part (''Upper Series''). The grade of M2 metamorphism increases from greenschist facies rocks containing relict M1 high-pressure assemblages at the top of the sequence to upper amphibolite facies rocks in the core (Jansen and Schuiling 1976; Feenstra 1985; Avigad 1998). Peak M2 conditions in the leucogneiss core have been estimated at $6–7 \pm 2$ kbar, $670–700 \pm 50$ °C (Jansen and Schuiling 1976; Buick 1988; Buick and Holland 1991). Heating and decompression is recorded by kyanite-bearing M2 pelitic assemblages of the leucogneiss core (Buick and Holland 1989). These assemblages are associated with S-C fabrics interpreted to show that metamorphism took place during ductile extension in a shallowly northward-dipping crustal-scale shear zone (Urai et al. 1990; Buick 1991).

K–Ar and $^{40}Ar/^{39}Ar$ dating of hornblende from the M2 biotite–chloritoid zone (~520 ± 20 °C; Jansen and Schuiling 1976) gave ages of 21.3 ± 0.6 and 19.8 ± 0.2 Ma, respectively (Andriessen et al. 1979; Wijbrans and McDougall 1988). These ages may be taken as the best estimate for the time of peak M2 metamorphism. Swarms of Early Miocene (19–20 Ma; Andriessen et al. 1991) aplites and pegmatites originate in the leucogneiss core and cross-cut peak M2 structures within it and in the Lower Series (Jansen 1977; Urai et al. 1990). These aplites and pegmatites are interpreted to have formed as the result of crystallization of melts produced during M2 metamorphism and in situ anatexis (Andriessen et al. 1991; Matthews et al. unpublished). Localized extensional deformation continued under retrograde M2 conditions and during the intrusion of a post-metamorphic granodiorite (13.6–12.1 Ma; Wijbrans and McDougall 1988) and led to the tectonic emplacement of unmetamorphosed Tertiary sedimentary units (tectonosedimentary unit in Fig. 1) onto both the granodiorite and the metamorphic complex (Lister et al. 1984; Gautier et al. 1993; John and Howard 1995).

Ultramafic rocks within the Naxos metamorphic complex

Ultramafic horizons occur at four different structural levels within the metamorphic sequence of Naxos. The deepest two levels are of interest in this study: (1) the Main Ultramafic Horizon (MUH) occurring within high-grade rocks at the boundary between the leucogneiss core and the Lower Series, (2) the Agia Ultramafic Horizon (AUH) occurring in northwest Naxos within sillimanite-grade rocks of the Lower Series. Ultramafic horizons at higher structural levels (in upper parts of the Lower Series and in the Upper Series) show textural, geochemical, and isotopic evidence for pre-metamorphic low-temperature serpentinization on the seafloor (Katzir et al. 1999). In contrast, petrologic and geochemical analysis of pre-M2 and M2 assemblages has shown that the MUH and AUH horizons are mantle flakes emplaced at depth into the subducted continental section of Naxos during collision and M1 metamorphism (Katzir et al. 1999). Similarity in peak metamorphic conditions and structural concordance of the ultramafic rocks and the country rocks indicates that the ultramafics were exhumed and experienced the M2 metamorphism with their host felsic rocks.

Field-relations, petrology, and thermobarometry of the ultramafic rocks

Main Horizon of meta-Ultramafic rocks (MUH)

The stratigraphically lowermost horizon of ultramafic rocks is composed of massive to moderately foliated, medium to coarse-grained meta-peridotites. The meta-peridotites are exposed as 1–10-m-size lenses enveloped by several meter-thick, highly foliated metasomatic monomineralic zones (blackwalls) that developed at the contacts between the meta-peridotite bodies and the sillimanite gneiss country rock. The most common order of metasomatic zoning from host felsic gneiss to meta-peridotite lens is: phlogopite – actinolite – anthophyllite (Jansen 1977). Locally, the metasomatic process has sometimes completely obliterated the peridotites, leaving blackwalls as the only indication of the previous occurrence of an ultramafic protolith. The petrographic and mineral compositional data is taken from four localities where relatively unmetasomatized meta-peridotites survive: (I) west of Koronos Peak, (II) north of Keramoti village, (III) east of Kourounochorio village,

and (IV) on the old cobbled path between the villages of Keramoti and Kinidharos (Fig. 1). Detailed descriptions of the petrography, mineral chemistry, and textures are given in Katzir et al. (1999) and here we present key features that form the basis for the P–T estimates and the stable isotope study.

Synkinematic recrystallization of the MUH peridotites under upper amphibolite facies conditions is indicated by the preferentially elongated, medium-grained assemblage of olivine (≥50% modally; $Fo_{90–92}$), orthopyroxene ($En_{90–93}$), Ca-amphibole (tremolite to Mg-hornblende), chlorite, and Cr–Al spinel (cf. Trommsdorff and Evans 1974; Evans 1977). This paragenesis includes the equilibrium assemblage for the dehydration reaction of Mg-chlorite: clinochlore ↔ forsterite + 2 enstatite + spinel + $4H_2O$. Reaction textures and prograde compositional zoning in the spinel (Fig. 2a) are indicative of a prograde reaction (Evans and Frost 1975; Frost 1991). Peak M2 temperatures in the leucogneiss core are constrained by the absence of staurolite and K-feldspar and the occurrence of muscovite and sillimanite in incipiently melted meta-pelites (Buick and Holland 1991; Katzir et al. 1999). At peak M2 pressures of 6 to 8 kbar, the relevant univariant reactions limit temperatures to 640–700 °C (Fig. 3). These peak M2 temperature estimates are consistent with the occurrence of spinel in the ultramafic assemblages (Fig. 3).

Relics of an older, higher-grade meta-peridotite precursor to the M2 assemblages are well preserved (Fig. 2b) as porphyroclasts of enstatite and forsterite randomly oriented within the M2 recrystallized matrix and showing strong undulose extinction. The pre-kinematic enstatites have high-Al_2O_3 and high-CaO cores (up to 5.5 and 0.9 wt%, respectively) and contain aligned exsolution lamellae of Cr-spinel. Other relics of the pre-M2 higher-grade peridotite include rare grains of high-Al

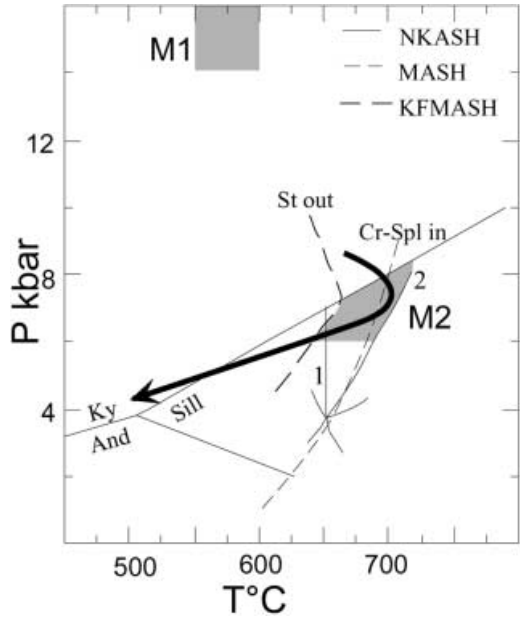

Fig. 3 P–T path for the leucogneiss core, Naxos. Minimum M1 conditions and peak M2 conditions are shown as *stippled* regions. M1 conditions are estimated by down-section extrapolation from jadeite blueschists in southeast Naxos (Avigad 1998). Peak M2 conditions are limited by pressure estimates of Buick and Holland (1989) and by univariant reactions: "staurolite out" (St + Ms + Qtz = Grt + Al-silicate + Bt + H_2O), Sill = Ky and "muscovite dehydration melting" (Ms + Ab + Qtz = Kfs + Al-silicate + melt; labeled *2*). Also shown are univariant reactions around an invariant point in the NKASH system (*short lines*) including the reaction by which incipient melting of wet meta-pelites is suggested to have occurred (Ms + Ab + Qtz + H_2O = Al-silicate + melt; labeled *1*; Buick and Holland 1991). The univariant line for the dehydration of chlorite to form Cr-spinel (Chl = Fo + En + Spl + H_2O) occurs within the peak M2 field. Equilibria in the NKASH system are taken from Buick and Holland (1991). All other calculations are made using the software Thermocalc version 2.7 (Holland and Powell 1998)

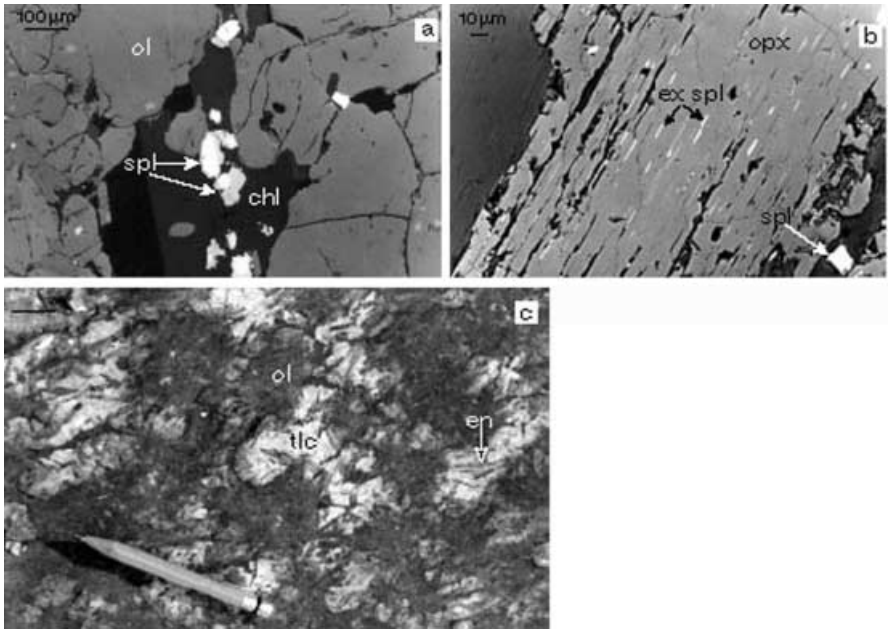

Fig. 2a, b Back-scattered electron images of the MUH meta-peridotites. **a** Polygonal mosaic of olivine dominates the peak M2 assemblage in Koronos meta-peridotite. A plate of chlorite (*black*) is overgrown by neo-formed spinel, which is zoned from Cr-rich cores (*white*) to Al-rich rims (*gray*); **b** pre-kinematic porphyroclast of orthopyroxene with exsolution lamellae of Cr-spinel set in M2-crystallized matrix (Kourounochorion meta-peridotite). **c** Field photograph of Agia mottled peridotite: randomly alternating light domains of talc + enstatite and dark domains of olivine. Pencil is 9 cm long. Abbreviations: *chl* chlorite, *en* enstatite, *ex spl* exsolved spinel, *ol* olivine, *opx* orthopyroxene, *spl* spinel, *tlc* talc

green spinel (60 wt% Al_2O_3) found at locality III (Kourounochorio). Aluminum- and Ca-in-Opx thermometry (Gasparik and Newton 1984; Brey and Köhler 1990) of relict orthopyroxene, olivine, and spinel yields temperatures of 1,050 ± 20 °C.

The thermometry, and petrographic and mineralogical relations thus suggest that mantle peridotites equilibrated in the spinel lherzolite field, cooled to at least upper amphibolite facies conditions and were incorporated into the Naxos continental section prior to the M2 event (Katzir et al. 1999). They were then isofacially metamorphosed along with the country rocks during M2.

Agia Ultramafic Horizon (AUH), northwest Naxos

This 50–70-m-thick ultramafic horizon is intermittently exposed for over 3 km within sillimanite grade rocks of the Lower Series (Fig. 1). A section across the horizon in a road-cut southwest of the abandoned village of Agia (25°31'E 37°11' N) is given in Fig. 4. Moving up-section from south to north, the northwest-dipping Lower Series gneisses are juxtaposed by a steep fault plane against the meta-peridotite. The meta-peridotite is intruded by 2-m-thick leucogranitic dike 20 m north of the fault. The dike is texturally zoned from a tourmaline and garnet-bearing aplitic core through tourmaline-rich pegmatitic margins to a tourmaline skarn bordering the peridotite. Further up-section, the northern part of the road-cut features NW-dipping alternating meter-scale slices of Lower Series gneisses and anthophyllite blackwalls, separated by thin actinolite blackwalls. This part of the section is also intruded by discordant 0.5-m-thick pegmatite dikes.

The lower contact of the peridotite is best exposed at a dry river-bed west of Agia. Thick anthophyllite blackwall (10–15 m) separates the meta-peridotite from the host gneisses. Metabasic pods, consisting of hornblende and plagioclase, occur at the transition from the anthophyllite blackwall to the meta-peridotite. Locally, these rocks display a complex pattern of zoning that includes clinozoisite-rich core surrounded by a chloritic rind charged with idioblasts of garnet, green spinel, magnetite, and blue-green amphibole. The AUH is not intruded by leucogranitic dikes at the river-bed exposure; however, up to 2–3-m-thick dikes are plentiful in the adjacent country rocks.

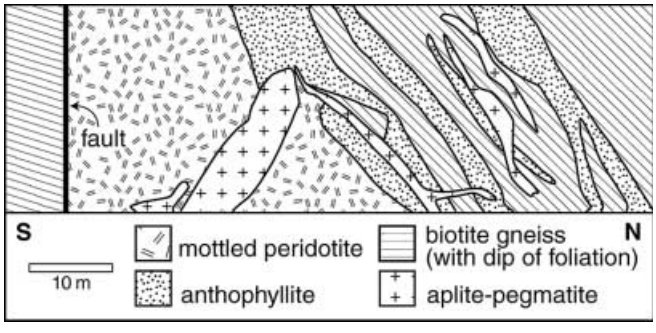

Fig. 4 North–south cross section of the AUH at a road-cut in 25°31'E, 37°11'N. The true dip of the host biotite gneisses is to the northwest

The country rocks are mainly dark biotite-rich felsic gneisses, consisting mainly of quartz, plagioclase, K-feldspar, biotite, hornblende, and epidote. Biotite and hornblende define a well-developed penetrative foliation indicating synkinematic crystallization at peak M2 conditions. Biotite replaces hornblende in places and forms shear bands that cut the main foliation and overprint the high-grade fabric. Post-M2 deformation is also seen in pelitic schists where extreme grain size reduction, shear bands and mica-fish structures form S-C mylonites.

The ultramafic rock exposed at Agia is a very coarse grained, mottled peridotite composed of randomly alternating dark- and light-colored domains (Fig. 2c). There is no evidence of schistosity development or preferred orientation of the minerals. The dark domains consist of 2–3-cm-long rectangular crystals of olivine ($Fo_{90–94}$) whereas the light parts consist of yellowish, long prisms (up to 4 cm) of orthopyroxene ($En_{91–93}$) within a fine-grained (100 μm) talc matrix. Olivine is black due to minute inclusions of magnetite that accompanies late serpentine in cracks. Textural relicts preserved within the olivine and orthopyroxene include: (1) coarse-grained olivine containing pockets of fine-grained, well-elongated chlorite, spinel, and enstatite; the texture and mineral composition of this relict Chl–Sp–En assemblage resemble those of the equivalent peak M2 assemblage in the MUH; (2) exsolved spinel occuring within coarse-grained enstatite. Sprays of anthophyllite needles ($Ath_{0.89}$, up to 0.5 cm long) overgrow both olivine and talc + orthopyroxene domains, thus post-dating the development of the mottled texture.

The silica-enriched AUH assemblages could have been derived from rocks that were previously enriched in silica by pre-metamorphic serpentinization. However, textural arguments do not favor this latter proposal. The coexistence of enstatite and talc in textural equilibrium, the presence of olivine inclusions within both idioblastic enstatite and talc matrix, the replacement of olivine by enstatite and talc, and the higher than normal peridotitic silica contents (e.g., 45–48 wt% SiO_2 for 40 wt% MgO; Katzir et al. 1999) suggest that the talc + enstatite assemblage formed at the expense of precursor olivine by the SiO_2 infiltration metasomatic reaction: 2 forsterite + $3SiO_2$ (aq) + H_2O ↔ enstatite + talc. This suggests that silica-rich aqueous fluids infiltrated into the peridotite, forming the white talc + enstatite domains in areas of relatively high silica activity, and causing recrystallization of olivine in areas where the activity of silica in solution was lower. The talc + enstatite paragenesis is stable either on the high-pressure or low-temperature side of the fluid-absent reaction, talc + 4 enstatite ↔ anthophyllite (Greenwood 1971; Chernosky et al. 1985). The late anthophyllite overgrowth could have occurred during the decompression and cooling that followed the peak of metamorphism and the silica-metasomatism event (Fig. 5).

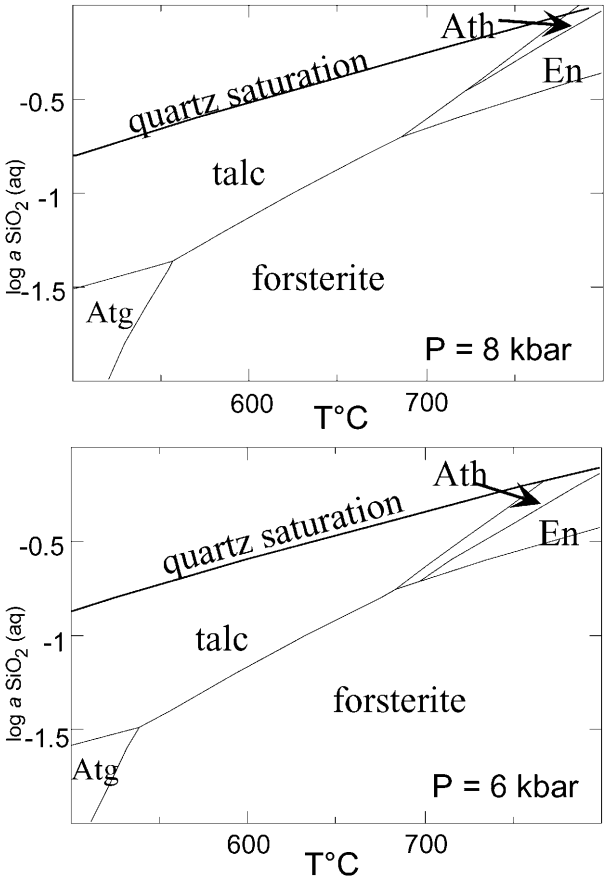

Fig. 5 Temperature vs. log a SiO_2(aq) for the MSH system at 8 and 6 kbar. Calculations are made using Thermocalc 2.7 (Holland and Powell 1998)

Two major stages of crystallization are thus evident in the Agia meta-peridotite: (1) a major infiltration event involving hydration and silica metasomatism that resulted in the development of the olivine and talc–enstatite domains; (2) retrograde anthophyllite crystallization post-dating the silica infiltration event. Ductile deformation in the Lower Series of Naxos climaxed at peak M2 temperatures (Urai et al. 1990; Buick 1991), and is well seen in the felsic gneisses and pelitic schists adjacent to the Agia peridotite in the form of strong penetrative foliation. The lack of evidence for ductile deformation during the crystallization of Agia meta-peridotite mineral assemblage suggests that the siliceous fluid-infiltration event post-dated peak M2 conditions. Both of the major AUH recrystallization stages thus occurred under retrograde conditions.

The evolution of ultrabasic assemblages during the infiltration of Si-rich fluids in Agia can be modeled on a log $a_{SiO2(aq)}$ vs. T diagram for the MSH system (Fig. 5). The diagrams were calculated for the pure Mg end members to avoid the imperfectly known effect of iron (Evans and Trommsdorff 1974; Frost 1975; Evans and Guggenheim 1988), and thus approximate maximum temperature conditions. At 8 kbar anthophyllite is only stable at T≥720 °C and cannot directly overprint forsterite. Talc, enstatite, and forsterite share, however, an invariant point. A decrease in pressure to 6 kbar lowers the temperature range of anthophyllite stability and places its field between talc and enstatite, thus sharing a join with forsterite. Taken together, the two diagrams suggest that at higher pressures talc + enstatite and forsterite will be stable mostly depending on $a_{SiO2(aq)}$. Reduction in pressure will stabilize anthophyllite at the expense of talc and enstatite and even forsterite if silica activity increases.

Oxygen isotope composition

MUH and AUH meta-peridotites

The oxygen isotope analyses of minerals are given in Table 1 and plotted in Fig. 6. The $\delta^{18}O$ values of minerals from the MUH peridotites are tightly grouped and show systematic differences for individual mineral species: olivine = 5.0 to 5.4‰, Ca-amphibole = 5.4 to 5.9‰, and orthopyroxene = 6.0 to 6.7‰. This sequence of $\delta^{18}O$ values is in accord with theoretical, experimental, and empirical studies of oxygen isotope fractionation (Zheng 1993a, 1993b; Mattey et al. 1994a, 1994b; Rosenbaum et al. 1994), but the fractionations between minerals are larger than those occurring at mantle temperatures (Fig. 6). Figure 6 shows the range of $\delta^{18}O$ values for olivine and the olivine–orthopyroxene fractionation in mantle xenoliths (Mattey et al. 1994a, 1994b). Ten out of eleven olivine analyses from the MUH plot within the range of mantle olivine values; however, Ca-amphibole and orthopyroxene values are higher than their respective mantle ranges. Olivine is modally the most abundant mineral and therefore the largest reservoir of oxygen in the peridotites. Thus, the larger than mantle $\Delta^{18}O_{(mineral–olivine)}$ values given by the dataset suggest that oxygen isotope exchange has occurred at metamorphic temperatures (e.g., 700 °C) rather than at mantle temperatures of 1,200 °C. Two samples of pre-M2 relict orthopyroxene have $\delta^{18}O$ values of 5.88 and 5.94‰, and are very close to the average mantle value, suggesting preservation of the isotopic signature acquired at mantle temperatures.

Minerals from the AUH meta-peridotites have a remarkably different isotopic composition from those of the MUH, characterized by high $\delta^{18}O$ values: 11.0 to 12.2‰ for olivine and 12.9 to 13.9‰ for orthopyroxene. These values indicate that recrystallization of both the olivine and talc–enstatite domains of the mottled peridotite occurred in the presence of fluids with higher $\delta^{18}O$ than found in the MUH ultramafics. Potential sources for such high-$\delta^{18}O$ fluids include the host Lower Series psammitic gneisses and the aplite–pegmatite dikes.

Blackwalls, host gneisses, and aplites/pegmatites

Tables 2 and 3 list the $\delta^{18}O$ values of minerals from blackwalls, country rocks, and aplite–pegmatite dikes

Table 1 Values of $\delta^{18}O$ of minerals from the meta-peridotites of the Main and Agia Ultramafic Horizons on Naxos, Greece. *r* relict; numbers of analyses are given in parentheses

Sample no.	Olivine	Orthopyroxene	Ca-amphibole	Others
Main Ultramafic Horizon				
Koronos				
NK 110	5.27 ± 0.18 (2)	6.19	5.45 ± 0.04 (2)	Opx (r) 5.88
NK 117	5.26	6.02	5.50	–
Keramoti				
NK 124	5.34 ± 0.20 (4)	6.66 ± 0.05 (3)	6.34	–
Kourounochorion				
NK 166	5.18 ± 0.12 (3)	6.29	–	–
NK 169	5.22	–	5.95	Opx (r) 5.94
NK 169–1	5.04 ± 0.05 (2)	–	5.74	–
NK 169–2	5.04 ± 0.08 (2)	–	5.81	–
Kinidharos				
NK 233–1	5.09	–	–	–
NK 314	5.35	–	–	–
NX 17	5.43 ± 0.08 (2)	–	–	–
NX 18	5.90	–	6.86	–
NX 15	5.16	–	–	–
Agia Ultramafic Horizon				
Agia road-cut				
NA 5	11.78 ± 0.13 (2)	13.66	–	–
Agia dry river-bed				
NA 187	12.24 ± 0.09 (3)	13.87 ± 0.20 (4)	–	–
NA 193	11.67	13.25 ± 0.09 (2)	12.79	–
NA 194	11.48	13.14	–	–
NA 798	11.03 ± 0.23 (2)	12.88 ± 0.04 (2)	–	–

associated with the meta-peridotites at Koronos and Kinidharos (MUH) and Agia (AUH). The blackwall minerals at each locality (Ath, Act, and Phl) define specific $\delta^{18}O$ ranges: 4.5 to 8.1‰ at Koronos, 7.8 to 9.5‰ at Kinidharos, and 13.4 to14.0‰ at Agia, respectively. Composed exclusively of hydrous minerals, the formation of the blackwalls must have involved addition of H_2O. The metasomatic zonation adjacent to Koronos meta-peridotite was studied in detail to evaluate the timing of the metasomatism. Figure 7 is a lithological map of the southern contact between the Koronos body and the host felsic gneiss, showing sampling sites and $\delta^{18}O$ values of mineral samples. The geometry of the Koronos blackwall is more complex than the relatively simple Ath–Act–Phl sequence described by Jansen (1977). A 2–5-m-thick anthophyllite reaction zone occurs at the gneiss–peridotite contact and is discordantly intruded by an aplite–pegmatite vein. The aplite margins are coated with centimeter-thick blackwalls of phlogopite. The anthophyllite blackwall also contains up to 10-cm-thick concordant and discordant layers of phlogopite and actinolite, which possibly represent desilicified and metasomatized syn- to post-kinematic aplitic veins. The Koronos blackwall thus formed by several metasomatic events, starting with peak M2 metasomatism and continuing until after the intrusion of the aplite veins.

To constrain the origin of the metasomatic fluids we have calculated the $\delta^{18}O$ of water in equilibrium at 650 °C with olivine of the peridotite lens, quartz of the host gneiss, and anthophyllite, actinolite, and phlogopite of the blackwall at the three localities (Table 4). The fractionation factors used in these calculations were derived by combining the mineral–calcite fractionations with the calcite–water calibration of O'Neil et al. (1969; data sources are given in the caption to Table 4).

The blackwall minerals at Koronos and Kinidharos give similar $\delta^{18}O$ values indicating that they grew in equilibrium from the same fluid. This is also supported by the fact that $\Delta^{18}O_{(Ath–Act)}$ of actinolite within MUH anthophyllite blackwalls is 0.4–0.8‰ and consistent with the predicted value of 0.6 for $\Delta^{18}O_{(Ath–Act)}$ at 640 °C (Kohn and Valley 1998a). A slight gradient in the isotopic composition is indicated by four samples of anthophyllite from a 2 m, north–south traverse from gneiss to peridotite at Koronos (Fig. 7), which shows a monotonic increase in $\delta^{18}O$ from 7.44‰ at the gneiss contact to 8.08‰ at the peridotite contact. The blackwall fluids have higher $\delta^{18}O$ values than the waters in equilibrium with the host-rock quartz or the M2 peridotite, indicating an additional fluid component. This could possibly be from nearby pelitic rocks or waters derived from aplite veins, which have slightly higher $\delta^{18}O$ than the blackwall water (Table 4).

The isotopic composition of Koronos phlogopite varies considerably from 7.4‰ in the monomineralic vein bordered by actinolite to 4.0–6.3‰ at the aplite blackwall where it coexists with quartz and feldspar. These differences can be explained by different degrees of isotopic re-equilibration. Monomineralic veins have no minerals with which they can undergo retrograde re-equilibration, whereas the phlogopite coexisting with

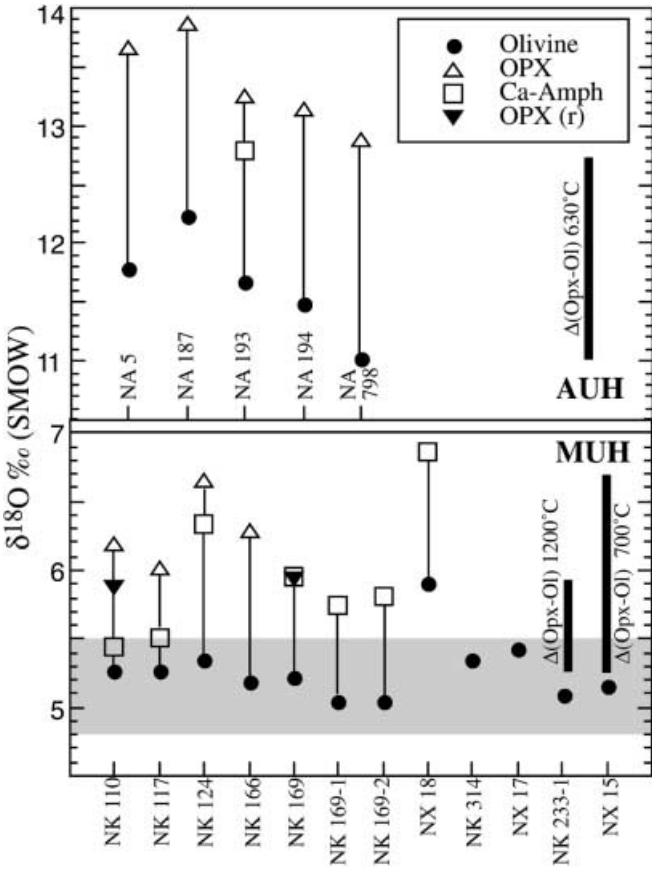

Fig. 6 Oxygen isotope fractionations of minerals from the MUH and AUH meta-peridotites. The analytical uncertainty is smaller than symbols. Note the different $\delta^{18}O$ scales for the MUH and the AUH. The *stippled band* at $\delta^{18}O = 5.20 \pm 0.35‰$ indicates the oxygen isotope composition of mantle olivine (Mattey et al. 1994a). The expected $\Delta^{18}O_{(Opx–Ol)}$ values at 630, 700, and 1,200 °C (Rosenbaum et al. 1994) are shown as *bars on the right*; *r* relict

quartz and feldspar will experience resetting because of its low closure temperature for diffusional exchange (270 ± 30 °C, Fortier and Giletti 1991).

The $\delta^{18}O_{water}$ values in equilibrium with the olivine of the recrystallized peridotite and the anthophyllite and actinolite of the blackwall in the AUH are similar at 15.1‰. This value matches $\delta^{18}O_{water}$ in equilibrium with quartz from the aplites and pegmatites of the AUH (14.9‰), but is 2.3‰ lower than the calculated $\delta^{18}O_{water}$ derived from the host gneisses. These results suggest that the peridotite and blackwall in Agia equilibrated with fluids derived from aplites and pegmatites.

Aplite veins intruding the ultramafic blackwalls at Koronos and Kinidharos show limited $\delta^{18}O$ variations among veins and within individual veins: quartz = 10.6 to12.0‰, tourmaline = 8.8 to10.2‰ and plagioclase = 8.4 to10.0‰.The aplite–pegmatite dike that intrudes the mottled peridotites in Agia has significantly higher $\delta^{18}O$ than the MUH aplite veins: $\delta^{18}O_{Qtz}$ = 15.5 to 15.8‰, $\delta^{18}O_{Tur}$ = 12.8 to 14.2‰, and $\delta^{18}O_{Grt}$ = 11.8 to 13.2‰ (Table 3). The variations in the $\delta^{18}O$ of the aplite–pegmatite dikes are considered to reflect isotopic exchange between the dike melts and their respective host rocks (Matthews et al. unpublished).

Discussion

Oxygen isotope thermometry

Oxygen isotope ratios for olivine–orthopyroxene pairs from the meta-peridotites of the MUH and AUH are plotted on a δ–δ diagram in Fig. 8. Isotherms plotted in the diagram are from the calibration of Rosenbaum et al. (1994). $\Delta^{18}O_{(Opx–Ol)}$ values in the MUH peridotites vary from 0.76 to 1.32‰ and form a steep trend bounded by the 700 and 1,200 °C isotherms (see inset to Fig. 8). This trend is interpreted to reflect partial exchange of oxygen isotopes between olivine and orthopyroxene during M2 metamorphism. Olivine, being more abundant than orthopyroxene in these MUH rocks, exhibits lower $^{18}O/^{16}O$ variability and almost no change from average mantle olivine value (5.20‰; Mattey et al. 1994a). Isotopic exchange is thus mostly reflected by increase in the $\delta^{18}O$ of orthopyroxene, as expected in a closed system (Gregory and Taylor 1986). The $\delta^{18}O$ values of the pre-M2 orthopyroxenes plot on the 1,200 °C isotherm, when paired with the $\delta^{18}O$ of olivine of the same rock samples, and define the mantle equilibration end member of the trend (Fig. 8).

The $\delta^{18}O$ values of olivine and orthopyroxene from the AUH plot along a linear equilibrium array (Fig. 8): $\Delta^{18}O_{(Opx–Ol)} = 1.72 \pm 0.14$. The linear correlation indicates isotopic equilibrium among the light and dark domains of the mottled peridotite and indicates complete recrystallization of both domains in the presence of the same infiltrating fluid. This linear correlation covers a relatively large and unusually high $\delta^{18}O$ range for ultramafic rocks (11–14‰). The mean fractionation of $\Delta^{18}O_{(Opx–Ol)} = 1.72 \pm 0.14$ corresponds to temperature of 630 ± 140 °C using the experimental calibration of Rosenbaum et al. (1994). Other calibrations yield lower average temperatures in the range of 530 to 570 °C (Kieffer 1982; Zheng 1993a; Mattey et al. 1994a). These temperatures agree well with the petrologic evolution of the AUH: crystallization of the mottled peridotite at post-peak M2 temperatures, constrained to 620–650 °C by the coexistence of staurolite and sillimanite in adjacent meta-pelites.

Values $\Delta^{18}O_{(Qtz–mineral)}$ of aplites and pegmatites in the MUH are highly scattered: $\Delta^{18}O_{(Qtz–Pl)}$ = 1.3 to 3.3‰, $\Delta^{18}O_{(Qtz–Phl)}$ = 3.9 to 7.1‰, and $\Delta^{18}O_{(Qtz–Tur)}$ = 1.6 to 3.0‰. "Apparent temperatures" calculated for quartz–mineral pairs give large ranges of 265–577 °C for plagioclase (Chiba et al. 1989), 278–543 °C for phlogopite (Chacko et al. 1996), and 357–621 °C for tourmaline (Kotzer et al. 1993). The highest temperatures of 540–670 °C overlap with peak M2 temperature estimates for the leucogneiss core and the MUH, and suggest that the large scatter in $\Delta^{18}O_{(Qtz–mineral)}$ values is the result of

Table 2 Values of $\delta^{18}O$ of minerals from blackwalls and country rocks associated with meta-peridotites of the Main and Agia Ultramafic Horizons

Blackwalls	Anthophyllite	Actinolite	Phlogopite
MUH			
Koronos			
NK 112	7.39	–	–
NK 114	6.02 ± 0.30 (2)	–	–
NK 121	–	7.12 ± 0.15 (4)	4.79 ± 1.00 (6)
NK 326	7.44	–	–
NK 327	7.74	–	–
NK 328	7.81	7.17	4.53
NK 328A	7.92 ± 0.04 (2)	–	–
NK 329	7.75	–	6.43
NK 330	–	–	7.41
NK 331	7.84	7.43	5.99
NK 332	7.95	7.49	4.53
NK 333	8.08	–	–
Kinidharos			
NK 75	8.48	7.85	8.87 ± 0.57 (2)
NX 21	8.35 ± 0.41 (2)	8.12	–
AUH			
Agia			
NA 182	–	13.78 ± 0.12 (2)	–
NA 183	13.80	–	–
NX 7	13.91	–	–
NX 8	–	13.46	–
NX 9	13.57	–	–
Country rocks	Quartz	Plagioclase	Biotite
Koronos			
NK 325 (orthogneiss)	8.55	–	–
Kinidharos			
NK 312 (orthogneiss)	9.81 (2)	7.71 ± 0.04 (2)	6.06 ± 0.16 (2)
Agia			
NX 1 (biotite gneiss)	17.69	–	–

Table 3 Values of $\delta^{18}O$ of minerals from leucogranitic dikes (aplites and pegmatites) intruding the Main and Agia Ultramafic Horizons and their associated phlogopite blackwalls

Sample no.	Quartz	Plagioclase	Tourmaline	Phlogopite
MUH				
Koronos				
NK 324	11.40	8.44	–	5.64
NK 335	11.14	–	–	4.04
NK 336	11.40 ± 0.38(2)	8.51	8.95 ± 0.11(2)	5.19
NK 337	–	–	–	6.26
Kinidharos				
NK 82	11.87 ± 0.01(2)	9.98	10.23	–
NK 92	–	–	9.10 ± 0.20(2)	4.20
NK 310 (1)	–	–	–	6.54
NK 310 (2)	11.64	8.78	–	7.48
NK 310 (3)	10.85	9.55	–	7.17 ± 0.01(2)
NK 310 (4)	11.64	9.82	–	6.84
NK 311 (1)	10.59	8.54	–	–
NK 311 (2)	11.68	8.43	–	–
NK 311 (3)	11.07	8.87 ± 0.02(2)	–	7.17
NK 311 (4)	10.92	–	–	6.94
NK 311 (5)	–	8.63	–	–
432–99	12.02	–	9.11	–
AUH				
Agia	Quartz	Tourmaline	Garnet	–
NA 6	15.69	–	11.85	–
NA 394	15.56	–	13.20	–
NA 395	15.85	14.19	–	–
NA 397	–	13.98	–	–
471–99	15.73	12.79	–	–

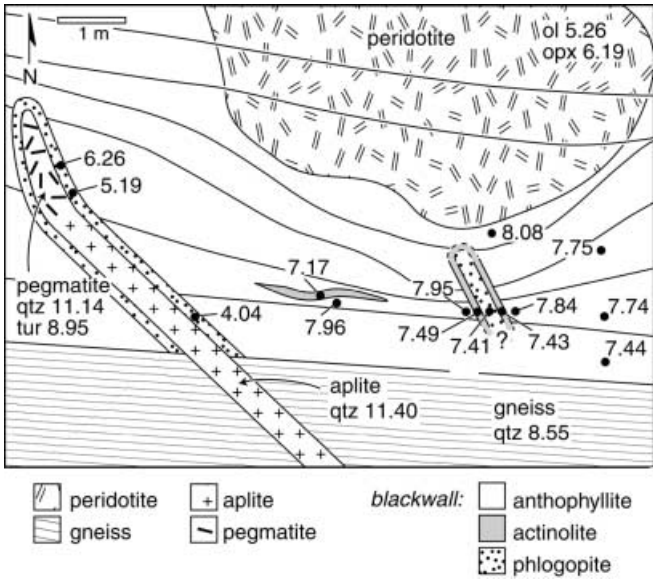

Fig. 7 Geological map of the southern contact between the Koronos meta-peridotite body (*I* in Fig. 1) and the host felsic gneiss, dominated by an anthophyllite blackwall. *Curved and straight lines* represent schistosity planes. Also shown are sampling sites (*black dots*) and $\delta^{18}O$ values of minerals. Abbreviations: *ol* olivine, *opx* orthopyroxene, *qtz* quartz, *tur* tourmaline

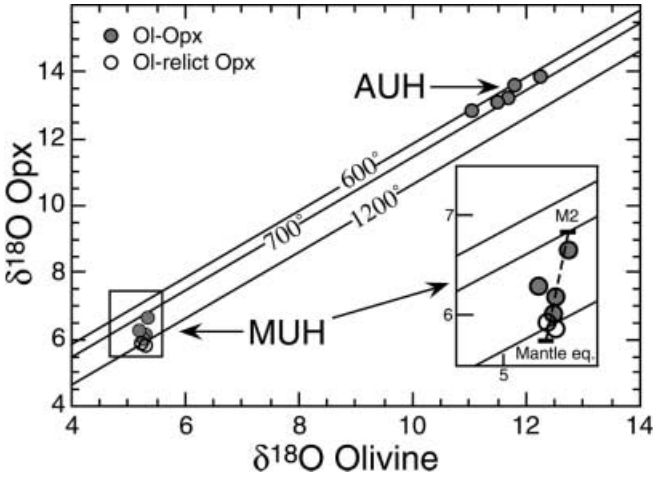

Fig. 8 Plot of $\delta^{18}O_{(orthopyroxene)}$ vs. $\delta^{18}O_{(olivine)}$ in the MUH and AUH meta-peridotites. Isotherms are calculated according to Rosenbaum et al. (1994). The analytical uncertainty is smaller than symbols

non-equilibrium oxygen isotope exchange during post-peak M2 cooling.

Prograde and retrograde fluid flow on Naxos

Meta-peridotites of both the MUH and the AUH were metamorphosed together with their host felsic gneisses under upper amphibolite facies conditions during the M2 event on Naxos. However, the resulting assemblages, the mode and intensity of deformation, and the oxygen isotope compositions of the two ultramafic horizons are surprisingly different. This dissimilarity calls for differences in the exact timing of crystallization within the M2 event and especially in the amount, origins, and pervasiveness of fluids involved in metamorphism. Petrologic relations (Fig. 3) and oxygen isotope thermometry (Fig. 8) show that the MUH meta-peridotite assemblages developed at peak metamorphic temperatures. Furthermore, the MUH peridotites show penetratively developed foliation aligned parallel to foliation in the country rocks indicating that they syn-kinematically crystallized at the peak of the M2 event (Fig. 7). During peak M2 recrystallization, the modally dominant mineral in the MUH meta-peridotites, olivine, retains mantle-like values of around 5.2‰, whereas Ca-amphibole and orthopyroxene show slightly higher values than their mantle ranges due to exchange at the metamorphic temperature. Both cation and oxygen isotope thermometry of pre-M2 orthopyroxene porphyroclasts give mantle equilibration temperatures. Thus, there is no marked change in the isotopic composition of the oxygen reservoir in the MUH peridotites during M2 metamorphism. Whole-rock major element studies also show that the MUH peridotites retain their original mantle composition, thus also excluding infiltration metasomatism during M2 (Katzir et al. 1999). The blackwalls that encircle the peridotites are metasomatic in origin. Since the MUH blackwalls are well foliated, the main phase of their growth occurred at prograde to peak M2 conditions. Infiltration of water along the peridotite–gneiss contact during prograde to peak M2 is thus inferred.

The preservation of penetratively deformed, recrystallized, yet unmetasomatized peridotites suggests that fluids were strongly channeled and volumes of fluid were relatively small. The petrologic, structural, and isotopic evidence indicates that internally buffered fluids coexisted with the MUH meta-peridotites during peak M2

Table 4 Calculated $\delta^{18}O$ (H_2O) in equilibrium at 650 °C. Mineral–water fractionations are calculated by combining the appropriate mineral–calcite fractionations with the Cc–H_2O calibration of O'Neil et al. (1969). Data sources: Qtz–Cc (Clayton et al. 1989); Fo–Cc (Chiba et al. 1989); Cc–Ath (combination of Cc–Di fractionation of Chiba et al. 1989; with Di–amphibole fractionations of Kohn and Valley 1998b); Cc–Phl (Chacko et al. 1996); Cc–Act/Tr (combination of Cc–Phl with Phl–Tr of Kohn and Valley 1998b). *bw aplite* blackwall adjacent to aplite dike

	Ol	Qtz (gneiss)	Ath	Act	Phl	Qtz (aplite)	Phl (bw aplite)
Koronos	8.8	7.7	9.0	9.0	9.1	10.4	7.0
Kinidharos	8.8	9.0	9.7	9.7	10.6	10.5	8.3
Agia	15.3	16.9	15.0	15.3	–	14.9	–

conditions. An internally buffered fluid evolution during prograde and peak M2 conditions was also inferred for the low-variance siliceous dolomite assemblages in the Lower Series (Baker and Matthews 1994). Buick and Holland (1991) suggested that the preservation of non-melted meta-pelites within the anatectic leucogneiss core was the result of lowered water activity due to partitioning of water into adjacent silicate melts. A plausible explanation for the peak-M2 rock-buffered fluid compositions and ratios in the MUH and the Lower Series is the contemporaneous presence of melt-phase in the leucogneiss core. The silicate melts, assisted by intense ductile deformation, became a major volatile reservoir for the deeper part of the Naxos sequence, and left only small volumes of fluid in the Lower Series to be buffered by minerals.

Retrograde M2 metasomatism of the AUH

Prograde and peak M2 penetrative foliation is well developed in all the lithologies of the Lower Series and is overprinted by local and narrow ductile shear zones as strain is partitioned into smaller volumes during retrograde metamorphism. In the AUH, S-C fabrics and extremely fine-grained mylonites overprint penetrative foliation within the host biotite gneisses and pelitic schists. Pegmatites that intrude the AUH blackwalls show mylonitic textures with fine-grained quartz ribbons wrapped around deformed feldspar porphyroclasts. However, the AUH peridotites preserve a randomly mottled coarse-grained texture and show no evidence for ductile deformation. Thus, unlike the MUH, the AUH mottled peridotites recrystallized at almost static, retrograde conditions. They might represent a kinematically inactive area among highly sheared domains and thus recrystallized during the post-peak M2 localized deformation. Peak M2 temperature estimates at AUH are 620–650 °C, based on the occurrence of staurolite and sillimanite in metapelite horizons, and the isotopic fractionations between olivine and enstatite indicate that they formed at peak metamorphic temperatures. Thus, structural, petrologic, and isotopic considerations suggest that AUH recrystallization occurred during the early part of M2 retrogression.

It was noted earlier that the mineral petrography of the AUH rocks are consistent with post-M2 metasomatism. However, the elevated $\delta^{18}O$ values and silica contents of the Agia peridotite, relative to the MUH peridotites, could also be the result of pre-metamorphic serpentinization. If the elevated $\delta^{18}O$ values of the AUH peridotites (11–14‰) were inherited from pre-metamorphic serpentinite, then hydration must have occurred at very low temperatures with either meteoric or sea water (Wenner and Taylor 1973) and high water volumes that resulted in complete serpentinization (Burkhard and O'Neil 1988). Several lines of evidence indicate that the AUH peridotites did not experience such near-surface complete serpentinization prior to metamorphism, and that the $^{18}O/^{16}O$-enrichment occurred during post-M2 Si-metasomatism.

1. The replacement of olivine by enstatite + talc and the presence of exsolved spinel within grains of enstatite indicates that olivine and enstatite were present in the peridotite prior to its recrystallization to form the mottled rock. The relict texture of fine-grained spinel and enstatite overgrowing chlorite, which is preserved within olivine of the AUH, is characteristic of prograde M2 metamorphism in the MUH peridotites. This peak M2 assemblage was shown to overprint pristine mantle peridotite in the MUH and its stabilization does not require previous serpentinization.
2. The AUH and the MUH peridotites have the same whole-rock chemical composition characteristics. The AUH and MUH peridotites form negative linear trends on major element variation diagrams with MgO as the fractionation index (Fig. 9). These trends are similar to those found in xenolith suites and Alpine-type peridotites and represent depletion processes caused by partial melt extraction from primitive upper mantle lherzolites. No evidence of serpentinization is suggested by the major element composition and trends of the AUH and the MUH peridotites. On the contrary, they support deep-seated emplacement of the peridotites into the Naxos continental sequence that did not involve serpentinization (Katzir et al. 1999).
3. Ultramafic rocks that were serpentinized prior to M2 metamorphism occur at higher structural levels at the exposures of Saggri and Ormos Agiasou (Fig. 1). These show relict serpentine textures overprinted by M2 assemblages. The whole-rock $\delta^{18}O$ values of these rocks are between 10.6 and 13‰. However, the textures and whole-rock chemical trends displayed by the Saggri and Ormos Agiasou and the AUH peridotites groups are completely different. Rocks from Ormos Agiasou and Saggri are highly enriched in SiO_2, depleted in MgO, and, most important, have almost no CaO (Fig. 9). Serpentinization involves partial to complete Ca loss of the precursor peridotite (Trommsdorff and Evans 1974; Coleman 1977). The AUH peridotites, however, have normal CaO contents, comparable to those of the MUH peridotites and other pristine, unaltered peridotites.

Thus, field, petrographic, petrologic, and geochemical arguments favor that the $^{18}O/^{16}O$-enriched AUH rocks developed during post-M2 Si-metasomatism. A number of observations link the metasomatism and crystallization of the mottled peridotites to the intrusion of aplitic–pegmatitic dikes into the Lower Series.

1. Leucogranitic aplite and pegmatite dikes are very abundant within the Lower Series sequence in northwest Naxos. Some of these dikes are up to 5 m thick and either cut or are close to the AUH. Direct evidence

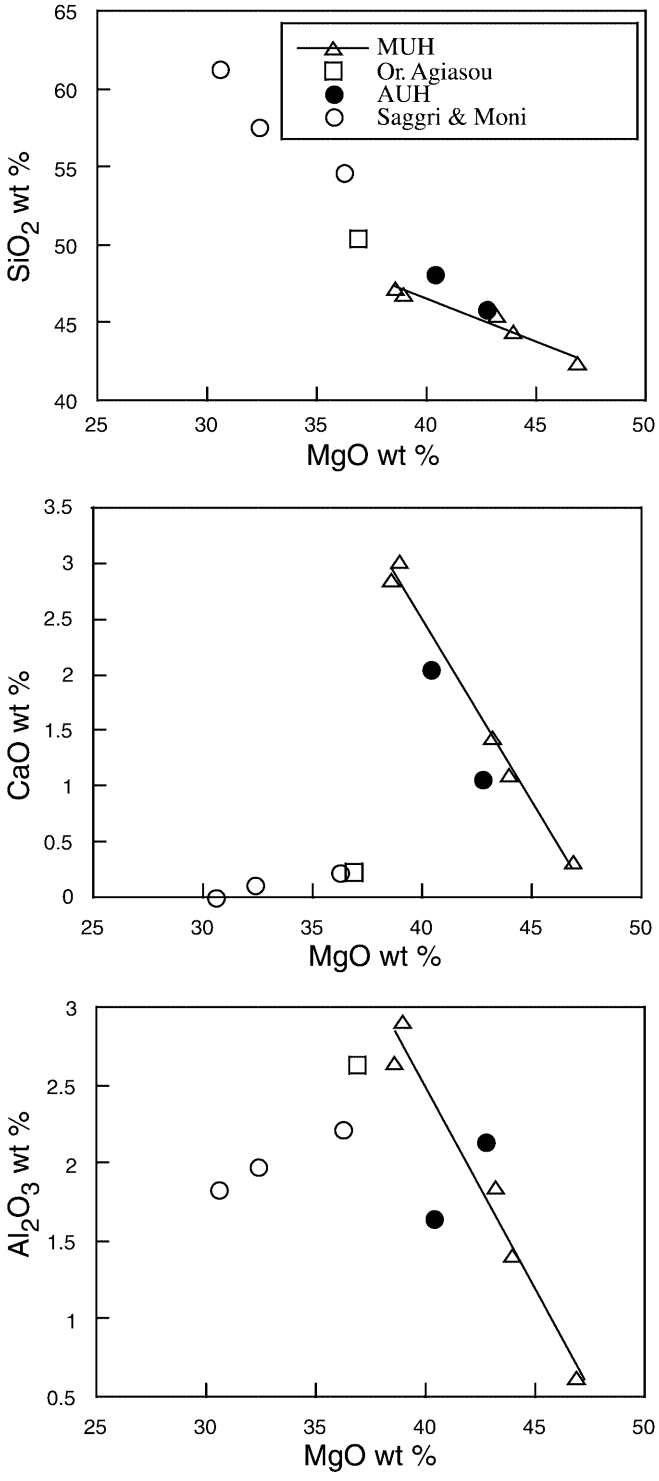

Fig. 9 Variation diagrams of SiO_2, CaO, and Al_2O_3 vs. MgO in ultramafic rocks of Naxos. (From Katzir et al. 1999)

of local exsolution of water from a leucogranitic dike is found in the thickest dike of the AUH road-cut exposure. The dike is zoned from aplitic core to pegmatitic margins, which suggests concentration of siliceous fluids close to the contact with the intruded peridotite. Monomineralic tourmaline skarn at the pegmatite–peridotite contact indicates extreme boron enrichment in fluids possibly expelled from the dike.

2. The high $\delta^{18}O$ values of the aplite–pegmatites in the AUH (Qtz = 15.5 to 15.8‰) match those of the AUH minerals and make them the most probable source for the $^{18}O/^{16}O$-enriched fluid involved in the formation of both light and dark domains of the mottled peridotites and the blackwalls. There is no other post-M2 fluid-rich source that could account for their oxygen isotope composition.
3. The metasomatic replacement of forsterite by talc + enstatite requires the introduction of considerable amounts of dissolved silica. Assuming $a_{H2O} = 1$ (based on the absence of magnesite in the mottled peridotites), and silica solubility of 2.3×10^{-3} in Si-saturated water, a minimum W/R ratio of approximately 80 (by weight) is calculated. Textures in the pegmatites determined petrographically and by cathodoluminescence include tourmaline growth zoning and at least two generations of quartz growth which suggest several stages of fluid-driven crystallization. The timing of the intrusion of the aplite dikes matches the post-peak M2 Si-metasomatism of the peridotites. K–Ar ages of aplitic tourmaline (19–20 Ma) are indistinct from K–Ar ages of hornblende in adjacent amphibolites, placing them contemporaneous with the M2 high-temperature event (Andriessen et al. 1991). The aplite–pegmatite dikes cut peak M2 structures but show extreme grain size reduction and mylonitic foliation in places (like in Agia) (Urai et al. 1990). These structural relations constrain the dike intrusion to post-peak M2 times.

Matthews et al. (unpublished) show that pegmatitic veins cross-cut anatectic melt textures in the leucogneiss core and terminate away from the core in the Lower Series (this is also seen in Fig. 7). Thus, pervasive infiltration of Si-rich fluids exsolved from aplites and pegmatites is an appropriate scenario for the AUH metasomatism. These fluids moved through host rocks of the Lower Series into the ultramafic rocks, which, being sensitive to Si-rich fluids, underwent metasomatic change. Anthophyllite blackwalls, which possibly formed earlier at peak M2 conditions, recrystallized during the retrograde fluid infiltration. The aplite–pegmatite dike swarms thus represent a fossil plumbing system that would have channeled aqueous fluids released from crystallizing melts in the leucogneiss core upwards into the Lower Series. These retrograde siliceous fluids metasomatized the AUH to form the mottled peridotite, and caused local recrystallization in the MUH blackwalls and in the calc-silicate assemblages of the Lower Series (Baker and Matthews 1994).

Acknowledgements We thank B. Hess for making thin sections, J. Fournelle for help with the electron microprobe, and O. Alef and A. Mor for help with mineral separation. This study was supported by NSF (EAR99/02973) and DOE (93ER14389). The research was also supported by Israel Science Foundation grant 455/00.

Y. Katzir is supported by an Albert and Alice Weeks post-doctoral fellowship of the Department of Geology and Geophysics, University of Wisconsin, Madison. Fieldwork was undertaken with the approval of the IGME, Athens. Reviews by L. Baumgartner and I. Cartwright greatly contributed to the improvement of this paper.

References

Andriessen PAM, Boelrijk NAIM, Hebeda EH, Priem HNA, Verdurmen EAT, Verschure RH (1979) Dating the events of metamorphism and granitic magmatism in the Alpine orogen of Naxos (Naxos, Greece). Contrib Mineral Petrol 69:215–225

Andriessen PAM, Banga G, Hebeda EH (1987) Isotopic age study of pre-Alpine rocks in the basal units on Naxos, Sikinos and Ios, Greek Cyclades. Geol Mijnbouw 66:3–14

Andriessen PAM, Hebeda EH, Simon OJ, Verschure RH (1991) Tourmaline K–Ar ages compared to other radiometric dating systems in Alpine anatectic leucosomes and metamorphic rocks (Cyclades and southern Spain). Chem Geol 91:33–48

Avigad D (1998) High pressure metamorphism and cooling on SE Naxos (Cyclades, Greece). Eur J Mineral 10:1309–1319

Avigad D, Garfunkel Z, Jolivet L, Azañon JM (1997) Back arc extension and denudation of Mediterranean eclogites. Tectonics 16:924–941

Baker J, Matthews A (1994) Textural and isotopic development of marble assemblages during the Barrovian-style M2 metamorphic event, Naxos, Greece. Contrib Mineral Petrol 116:130–144

Baker J, Matthews A (1995) The stable isotope evolution of a metamorphic complex, Naxos, Greece. Contrib Mineral Petrol 120:391–403

Baker J, Bickle MJ, Buick IS, Holland TJB, Matthews A (1989) Isotopic and petrological evidence for the infiltration of water-rich fluids during the Miocene M2 metamorphism on Naxos, Greece. Geochim Cosmochim Acta 53:2037–2050

Brey GP, Köhler T (1990) Geothermobarometry in four-phase lherzolite II. New thermobarometers, and practical assessment of existing thermobarometers. J Petrol 31:1353–1378

Buick IS (1988) The metamorphic and structural evolution of the Barrovian overprint, Naxos, Cyclades, Greece. PhD Thesis, University of Cambridge

Buick IS (1991) The late Alpine evolution of an extensional shear zone, Naxos, Greece. J Geol Soc Lond 148:93–103

Buick IS, Holland TJB (1989) The P–T–t path associated with crustal extension, Naxos, Cyclades, Greece. In: Daly JS, Cliff RA, Yardley BWD (eds) Evolution of metamorphic belts. Geol Soc Lond Spec Publ 43:365–369

Buick IS, Holland TJB (1991) The nature and distribution of fluids during amphibolite facies metamorphism, Naxos (Greece). J Metamorph Geol 9:301–314

Buick IS, Cartwright I, Williams IS (1997) High-temperature retrogression of granulite-facies marbles from the Reynolds Range Group, central Australia: phase equilibria, isotopic resetting and fluid fluxes. J Petrol 38:877–910

Burkhard DJM, O'Neil JR (1988) Contrasting serpentinization processes in the eastern Central Alps. Contrib Mineral Petrol 99:498–506

Cartwright I (1988) Crystallization of melts, pegmatite intrusion and the Inverian retrogression of the Scourian complex, northwest Scotland. J Metamorph Geol 6:77–93

Chacko T, Hu X, Mayeda TK, Clayton RN, Goldsmith JR (1996) Oxygen isotope fractionations in muscovite, phlogopite, tremolite and rutile. Geochim Cosmochim Acta 60:2595–2608

Chernosky JV, Day HW, Caruso LJ (1985) Equilibria in the system $MgO–SiO_2–H_2O$: experimental determination of the stability of Mg-anthophyllite. Am Mineral 70:223–236

Chiba H, Chacko T, Clayton RN, Goldsmith JR (1989) Oxygen isotope fractionations involving diopside, forsterite, magnetite, and calcite: applications to geothermometry. Geochim Cosmochim Acta 53:2985–2995

Clayton RN, Goldsmith JR, Mayeda TK (1989) Oxygen isotope fractionation in quartz, albite, anorthite and calcite. Geochim Cosmochim Acta 53:725–733

Clemens JD, Droop GTR (1998) Fluids, P–T paths and the fates of anatectic melts in the Earth's crust. Lithos 44:21–36

Coleman RG (1977) Ophiolites, ancient oceanic lithosphere? Springer, Berlin Heidelberg New York

Deines P, Haggerty SH (2000) Small-scale oxygen isotope variations and petrochemistry of ultradeep (> 300 km) and transition zone xenoliths. Geochim Cosmochim Acta 64:117–131

Eiler JM, Farley KA, Valley JW, Hofmann AW, Stolper EM (1996) Oxygen isotope constraints on the sources of Hawaiian volcanism. Earth Planet Sci Lett 144:453–468

Evans BW (1977) Metamorphism of Alpine peridotite and serpentinite. Annu Rev Earth Planet Sci 5:397–447

Evans BW, Frost BR (1975) Chrome-spinel in progressive metamorphism – a preliminary analysis. Geochim Cosmochim Acta 39:959–972

Evans BW, Guggenheim S (1988) Talc, pyrophyllite and related minerals. Miner Soc Am Rev Mineral 19:225–294

Evans BW, Trommsdorff V (1974) Stability of enstatite + talc, and CO_2-metasomatism of metaperidotite, Val d'Efra, Lepontine Alps. Am J Sci 274:274–296

Feenstra A (1985) Metamorphism of bauxites on Naxos. PhD Thesis, Rijks Universiteit, Utrecht, Netherlands

Fortier SM, Giletti BJ (1991) Volume self-diffusion of oxygen in biotite, muscovite, and phlogopite micas. Geochim Cosmochim Acta 55:1319–1330

Frost BR (1975) Contact metamorphism of serpentinite, chloritic blackwall and rodingite at Paddy-Go- Easy Pass, Central Cascades, Washington. J Petrol 16:272–313

Frost BR (1991) Stability of oxide minerals in metamorphic rocks. Miner Soc Am Rev Mineral 25:469–483

Fyfe WS (1973) The granulite facies, partial melting, and the Archean crust. Phil Trans R Soc Lond A273:457–461

Gasparik T, Newton RC (1984) The reversed alumina contents of orthopyroxene in equilibrium with spinel and forsterite in the system $MgO–Al_2O_3–SiO_2$. Contrib Mineral Petrol 85: 186–196

Gautier P, Brun JP, Jolivet L (1993) Structure and kinematics of Upper Cenozoic extensional detachment on Naxos and Paros (Cyclades Islands, Greece). Tectonics 12:1180–1194

Greenwood HJ (1971) Anthophyllite, corrections and comments on its stability. Am J Sci 270:151–154

Gregory RT, Taylor HP (1986) Non-equilibrium, metasomatic $^{18}O/^{16}O$ effects in upper mantle mineral assemblages. Contrib Mineral Petrol 93:124–135

Holland TJB, Powell R (1998) An internally consistent thermodynamic data set for phases of petrological interest. J Metamorph Geol 16:309–343

Jansen JBH (1977) The geology of Naxos. Geol Geophys Res 1, Institute of Geological and Mining Research (IGME), Athens

Jansen JBH, Schuiling RD (1976) Metamorphism on Naxos: petrology and geothermal gradients. Am J Sci 276:1225–1253

John BE, Howard KA (1995) Rapid extension recorded by cooling-age pattern and brittle deformation, Naxos, Greece. J Geophys Res 100:9969–9979

Katzir Y, Avigad D, Matthews A, Garfunkel Z, Evans BW (1999) Origin and metamorphism of ultrabasic rocks associated with a subducted continental margin, Naxos (Cyclades, Greece). J Metamorph Geol 17:301–318

Keay S, Lister G (1997) Inside the dome of the Naxos core complex. In: Lister G, Forster M (eds) Inside the Aegean metamorphic core complexes. Aust Crust Res Cent Tech Publ 45, pp 75–87

Kieffer SW (1982) Thermodynamic and lattice vibrations of minerals: 5. Applications to phase equilibria, isotopic fractionation, and high-pressure thermodynamic properties. Rev Geophys Space Phys 20:827–849

Kohn MJ, Valley JW (1998a) Oxygen isotope geochemistry of the amphiboles: isotope effects of cation substitutions in minerals. Geochim Cosmochim Acta 62:1947–1958

Kohn MJ, Valley JW (1998b) Obtaining equilibrium isotope fractionations from rocks: theory and examples. Contrib Mineral Petrol 132:209–224

Kohn MJ, Spear FS, Valley JW (1997) Dehydration-melting and fluid recycling during metamorphism: Rangley formation, New Hampshire, USA. J Petrol 38:1255–1277

Kotzer TG, Kyser TK, King RW, Kerrich R (1993) An empirical oxygen- and hydrogen-isotope geothermometer for quartz–tourmaline and tourmaline–water. Geochim Cosmochim Acta 57:3421–3426

Kyser TK, O'Neil JR, Carmichael ISE (1981) Oxygen isotope thermometry of basic lavas and mantle nodules. Contrib Mineral Petrol 77:11–23

Kyser TK, O'Neil JR, Carmichael ISE (1982) Genetic relations among basic lavas and ultramafic nodules: evidence from oxygen isotope composition. Contrib Mineral Petrol 81:88–102

Lamb WM, Valley JW (1984) Metamorphism of reduced granulites in a low-CO_2 vapor-free environment. Nature 228:45–50

Lister GS, Banga G, Feenstra A (1984) Metamorphic core complexes of Cordilleran type in the Cyclades, Aegean Sea, Greece. Geology 12:221–225

Mattey D, Lowry D, Macpherson C (1994a) Oxygen isotope composition of mantle peridotite. Earth Planet Sci Lett 128:231–241

Mattey DP, Lowry D, Macpherson CG, Chazot G (1994b) Oxygen isotope composition of mantle minerals by laser fluorination analysis: homogeneity in peridotites, heterogeneity in eclogites. Mineral Mag 58A:573–574

Matthews A, Baker, J, Mattey DP (2002) High temperature metamorphism in marbles as a consequence of volatile release from crystallizing anatectic melts, Naxos, Greece. Eur J Mineral (in press)

Olsen SN (1987) The composition and role of fluids in migmatites: a fluid inclusion study of the Front Range rocks. Contrib Mineral Petrol 96:104–120

O'Neil JR, Clayton RN, Mayeda TK (1969) Oxygen isotope fractionation in divalent metal carbonates. J Chem Phys 51:5547–5558

Reischmann T (1998) Pre-Alpine origin of tectonic units from the metamorphic complex of Naxos, Greece, identified by single zircon Pb/Pb dating. Bull Geol Soc Greece 32:101–111

Rosenbaum JM, Kyser TK, Walker D (1994) High temperature oxygen isotope fractionation in the enstatite–olivine–$BaCO_3$ system. Geochim Cosmochim Acta 58:2653–2660

Spear FS, Kohn MJ, Cheney JT (1999) P–T paths from anatectic pelites. Contrib Mineral Petrol 134:17–32

Spicuzza MJ, Valley JW, Kohn MJ, Girard JP, Fouillac AM (1998a) The rapid heating, defocused beam technique: a CO_2-laser-based method for highly precise and accurate determination of $\delta^{18}O$ values of quartz. Chem Geol 144:195–203

Spicuzza MJ, Valley JW, McConnel VS (1998b) Oxygen isotope analysis of whole rocks via laser-fluorination: an air-lock approach. Geol Soc Am Abstr Prog 30:80

Stevens G, Clemens JD, Droop GTR (1997) Melt production during granulite facies anatexis: experimental data from "primitive" metasedimentary protoliths. Contrib Mineral Petrol 128:352–370

Trommsdorff V, Evans BW (1974) Alpine metamorphism of peridotitic rocks. Schweiz Mineral Petrogr Mitt 54:333–352

Urai JL, Schuiling RD, Jansen JBH (1990) Alpine deformation on Naxos (Greece). In: Knipe RJ, Rutter EH (eds) Deformation mechanisms, rheology and tectonics. Geol Soc Lond Spec Publ 54:509–522

Valley JW, Bohlen SR, Essene EJ, Lamb W (1990) Metamorphism in the Adirondacks: II. The role of fluids. J Petrol 31:555–596

Valley JW, Kitchen N, Kohn MJ, Niendorf CR, Spicuzza MJ (1995) UWG-2, a garnet standard for oxygen isotope ratios: strategies for high precision and accuracy with laser heating. Geochim Cosmochim Acta 59:5523–5531

Valley JW, Kinny PD, Schulze DJ, Spicuzza MJ (1998) Zircon megacrysts from kimberlite: oxygen isotope variability among mantle melts. Contrib Mineral Petrol 133:1–11

Wenner DB, Taylor HP (1973) Oxygen and hydrogen isotope studies of the serpentinization of ultramafic rocks in oceanic environments and continental ophiolite complexes. Am J Sci 273:207–239

Wijbrans JR, McDougall I (1988) Metamorphic evolution of the Attic Cycladic metamorphic belt on Naxos (Cyclades, Greece) utilizing $^{40}Ar/^{39}Ar$ age spectrum measurements. J Metamorph Geol 6:571–594

Zheng YF (1993a) Calculation of oxygen isotope fractionation in anhydrous silicate minerals. Geochim Cosmochim Acta 57:1079–1091

Zheng YF (1993b) Calculation of oxygen isotope fractionation in hydroxyl-bearing silicates. Earth Planet Sci Lett 120:247–263